Thin Film Morphology in Triblock Terpolymers with One and Two Crystallizable Blocks

Adriana Boschetti-de-Fierro,[†] Lea Spindler,[‡,§] Günter Reiter,[‡] Dania Olmos,[⊥] Sergei Magonov,[#,||] and Volker Abetz*[,†]

Institute of Polymer Research, GKSS Research Centre Geesthacht GmbH, 21502 Geesthacht, Germany; Institut de Chemie des Surfaces et Interfaces, 15 rue Jean Starcky, F-68057 Mulhouse, Cedex, France; Departamento de Ciencia e Ingeniería de Materiales e Ingeniería Química, Universidad Carlos III de Madrid, 28911, Leganés, Madrid, Spain; and Veeco Instruments, Santa Barbara, California 93117

Received February 13, 2007; Revised Manuscript Received April 10, 2007

ABSTRACT: The thin film morphology of novel polybutadiene-*block*-polystyrene-*block*-poly(ethylene oxide) (PB-*b*-PS-*b*-PEO) and polyethylene-*block*-polystyrene-*block*-poly(ethylene oxide) (PE-*b*-PS-*b*-PEO) triblock terpolymers was determined by atomic force microscopy. The experiments were carried out on dry, wet, and heated samples in order to vary the contrast among the blocks. The different measurements allowed the discrimination between the PE and the PEO blocks, which was otherwise not possible. The effect of different thermal treatments (related to the crystallization temperatures) on the generated morphology was studied for a confined spherical morphology. The domain size, i.e., disk diameter, was found to increase as the crystallization temperature was increased.

Introduction

Block copolymers are widely studied materials. One of the reasons is that their properties depend on the properties of the constituent blocks and can therefore be tailored.[1−3] The second reason is their ability to self-assemble into microphases with dimensions in the nanometer range when the blocks are incompatible.[1−18] This allows the use of block copolymers in bulk as compatibilizers, dispersion agents, impact modifiers, and carriers.[8,19−22] Taking advantage of the surface properties, as in the case of thin films, they find applications as selective surfaces, patterning surfaces, and templates for nanotopography.[8,23−27] The complete characterization of a given block copolymer not only is based on its molecular properties but also comprises the determination of its morphology.

The process of self-assembly is thermodynamically based on the segmental interaction parameters between the constituent blocks, but it is also affected by the presence of any given surface, usually in the form of a substrate, a nanoparticle, or a crystal. Although there are a wide number of publications reporting morphological studies of diblock copolymers with one crystallizable block,[18,28−38] the analysis of more complex cases has been the topic of only few contributions.[39−51] For the simplest case, i.e., an amorphous diblock copolymer, the generated morphologies vary generally from disordered state to spheres, cylinders, cocontinuous gyroid, and lamella when the volume fraction of one block increases from 0 to 0.5.[1]

A variety of different fascinating morphologies arises when more than two blocks are included in the system. In the most simple case these are amorphous triblock terpolymers, where morphologies such as core−shell cylinders or core−shell gyroid are found.[52] Also, tetrablock quarterpolymers and higher systems have been reported.[53] Including a crystallizable block in the system will imply that the crystallization could occur within the microphase, or it could take over the microphase separation process and completely disrupt the self-assembly, which is known as break-out.[54] Furthermore, one can imagine the additional contribution of a second crystallizable block with lower T_c, which might interact with the already created crystal.

In order to address this interesting subject, we have synthesized polybutadiene-*block*-polystyrene-*block*-poly(ethylene oxide) (PB-*b*-PS-*b*-PEO) and polyethylene-*block*-polystyrene-*block*-poly(ethylene oxide) (PE-*b*-PS-*b*-PEO) triblock terpolymers by sequential anionic polymerization in different compositions. The corresponding morphological characterization in the bulk state was carried out by small-angle X-ray scattering and transmission electron microscopy.[39] Since none of the mentioned methods allows the discrimination between the two crystalline blocks, i.e., PE and PEO, the designation of the observed morphologies was not achieved. In this contribution, we use atomic force microscopy (AFM) in order to overcome this handicap and to achieve a complete morphological characterization, attaining the differentiation between the two crystalline blocks both by imaging wet surfaces (where the PEO blocks get swollen) and by temperature-dependent imaging (where the thermal transitions of each block can be identified). Since the AFM technique is used on thin films, in this contribution we also compare the bulk and thin film morphology. Finally, we applied different thermal treatments to our samples in order to modify the restrictions imposed by the surface and control the crystallization. In this simple way, the generated morphology is influenced.

Experimental Part

Materials. Polybutadiene-*block*-polystyrene-*block*-poly(ethylene oxide) (PB-*b*-PS-*b*-PEO) linear triblock terpolymers have been synthesized by sequential anionic polymerization, as described elsewhere.[39] Further catalytical hydrogenation produced polyethylene-*block*-polystyrene-*block*-poly(ethylene oxide) (PE-*b*-PS-*b*-PEO), a linear triblock terpolymer with two crystallizable blocks separated by a glassy middle block. Molecular characteristics of the triblock

* Corresponding author. E-mail: volker.abetz@gkss.de.
[†] GKSS Research Centre Geesthacht GmbH.
[‡] Institut de Chemie des Surfaces et Interfaces.
[⊥] Universidad Carlos III de Madrid.
[#] Veeco Instruments.
[§] Present address: Faculty of Mechanical Engineering, University of Maribor, Smetanova 17, Maribor, Slovenia.
[||] Present address: Agilent Technologies, 4330 Chandler Blvd., Chandler, AZ 85226.

10.1021/ma0703812 CCC: $37.00
Published on Web 06/21/2007

Table 1. Molecular Weight (M_n) of Each Block and Molecular Weight Distributions (M_w/M_n) of the Triblock Terpolymers;[39] the Content of 1,2-Units in the PB Block Is Given in Parentheses

	M_n (kg/mol)			
	PB[a] (%1,2[b])/PE[c]	PS[c]	PEO[c]	M_w/M_n
$B_{16}S_{68}EO_{16}^{210}/E_{17}S_{67}EO_{16}^{211}$	35 (11.5)/36	142	33	1.01
$B_{29}S_{40}EO_{31}^{168}/E_{29}S_{40}EO_{31}^{170}$	48 (12.9)/50	67	53	1.03
$B_{37}S_{16}EO_{47}^{76}/E_{38}S_{16}EO_{46}^{77}$	28 (11.8)/29	13	36	1.03

[a] Determined by size exclusion chromatography experiments in THF calibrated against PB standards. [b] Determined by ^{1}H NMR spectroscopy in $CDCl_3$. [c] Determined by ^{1}H NMR spectroscopy using the molecular weight of the PB precursor obtained by SEC in THF calibrated against PB standards.

terpolymers used in the present study are presented in Table 1. In the notation here employed, $A_xB_yC_z^m$, the subscripts stand for the mass fraction in percent and the superscript indicates the overall number-averaged molecular weight M_n of the block copolymer in kg/mol.

Transmission Electron Microscopy (TEM). The bulk morphology of PB-*b*-PS-*b*-PEO and PE-*b*-PS-*b*-PEO triblock terpolymers was studied by bright field TEM using a Zeiss CEM 902 electron microscope operated at 80 kV and a Tecnai G2 F20 electron microscope operated at 200 kV.[39] Films were prepared by casting from a 3 wt % hot (70 °C) toluene polymer solution. After 1 week the solvent was completely evaporated, and the films were slowly cooled to room temperature and dried under vacuum at room temperature for 24 h. Further annealing treatment was carried out under nitrogen flow, holding the samples at 120 °C for 6 h. Thin sections were cut at −130 °C with a Reichert-Jung Ultracut E microtome equipped with a diamond knife. The non-hydrogenated precursors were stained by exposure to OsO_4 vapor for 60 s, and the hydrogenated terpolymers were stained by exposure of the thin sections to RuO_4 vapor for 30−40 min.

Tapping Mode Atomic Force Microscopy. The images were taken on a "Digital Instruments" MultiMode AFM (NanoScope IV controller) operating in tapping mode at ambient conditions, using commercial silicon TM AFM tips (model MPP 12100) with a free resonance frequency in the range from 123 to 151 kHz and spring constants in the range from 5 to 10 N/m.

Thin films of PB-*b*-PS-*b*-PEO and PE-*b*-PS-*b*-PEO triblock terpolymers were prepared by spin-coating (2000 rpm, 20 s) from 10.0 mg/mL toluene solutions on cleaned polished silicon wafers. The silicon wafers were cleaned in a water-saturated UV-ozone atmosphere for at least 24 h. The spin-coated films were annealed at 200 °C under N_2 for 60 min, using a Linkam THMS 600 hot stage with TMS 91 controller. The annealing step was followed by different isothermal crystallization treatments. The resultant film under these conditions have thicknesses around 60−70 nm.

Swelling Experiments. Swelling experiments were performed on annealed thin films. A drop of Millipore water was deposited on the film after spin-coating and annealing 60 min at 200 °C. The excess of water was removed with a pipet after 30 min, and the sample was measured immediately.

Heating Experiments. The measurements at elevated temperatures were conducted with a commercial thermal accessory supplied by the microscope manufacturer. Heating of the sample, which was performed with a Pt-resistive element underneath the sample puck, was accompanied by heating of a probe. Such dual heating provides a more controlled sample temperature and stable tapping mode imaging at elevated temperatures up to 250 °C. Purging of a sample compartment with a light stream of He gas was arranged to prevent block copolymer oxidation at high temperatures.

Results and Discussion

Morphology Determination for $E_{17}S_{67}EO_{16}^{211}$. In images obtained by AFM measurements, the height image reflects the sample topography. Since the samples were prepared by spin-coating and later annealing, this image will give information related to the smoothness of the film and to the film morphology. However, the possibility of sample preparation effects and artifacts should be always considered. In the case of block copolymers with rubbery and glassy blocks, low-force conditions are those at which a tip properly tracks the sample surface. Otherwise, an assignment of height images features to surface topography might be misleading.[55]

In crystallizable block copolymers, the AFM phase mode gives very rich information due to the large difference in viscoelastic properties between crystalline and amorphous phases. On the basis of the nature of the blocks, the corresponding phase images will feature bright or white domains corresponding to a polyethylene or a poly(ethylene oxide) crystal. The dark domains correspond to the polybutadiene block or the amorphous part of either crystallizable block. The intermediate or gray domain will represent the polystyrene block, which stiffness is relatively high (when the block is below its glass transition temperature), although it is lower than the stiffness of any crystal.

The results of AFM imaging for the pair $B_{16}S_{68}EO_{16}^{210}/E_{17}S_{67}EO_{16}^{211}$ are presented in Figure 1. As can be seen from the data scale ($z_{max} = 20$ nm), the films are very smooth after the spin-coating and further thermal treatment. In the phase image presented in Figure 1c some crystalline lamellae can be identified inside the circular domains. However, from the AFM image alone it would not be possible to differentiate between the two crystallizable blocks, since the viscoelastic difference between two crystals does not give sufficient contrast. Analogously, one is also not able to differentiate between the two amorphous phases, which show up as low AFM phase materials (i.e., dark in the color scale).

In the phase image presented in Figure 1a, it is possible to distinguish some bright domains corresponding to crystalline spheres of poly(ethylene oxide), which despite its low crystallization temperature (presented in ref 39, $T_c = -33.8$ °C) has crystallized after long storage time, i.e., 20 months, at room temperature (the freshly prepared film did not present any phase contrast, results not shown). Within the crystalline domains it is not possible to identify crystalline lamellae (only a solid bright sphere is visible and the amorphous part is not resolved). The polybutadiene block remains unidentified in both height and phase images, which might indicate that it forms a layer most probably toward the air surface. The morphology of the hydrogenated $E_{17}S_{67}EO_{16}^{211}$ terpolymer is different (see Figure 1c). It is possible to see spherical domains filled with crystalline lamellae and amorphous phase. The polystyrene block forms the matrix for the spherical or disklike domains of the polyethylene and/or poly(ethylene oxide), which are the two blocks being able to undergo crystallization. However, in this system large supercoolings are required to initiate crystallization, as was presented elsewhere.[39] At this point, as has already been mentioned, it is not possible to differentiate between the two crystalline phases (or the two amorphous phases) based only on the presented AFM images.

Closer looks into the morphology are provided by imaging at a 500 nm window (Figure 1e) and a zoom-in into its phase image (Figure 1f). There, the inner domain structure is nicely observed. The supposed lamellae are observed as filling the domains by linking two points of the surface or being linked to the interface at one end and linked at another lamella at the other end. Actually, crystal nucleation from the surface is expected in this system, as observed by crystallization kinetic studies.[56]

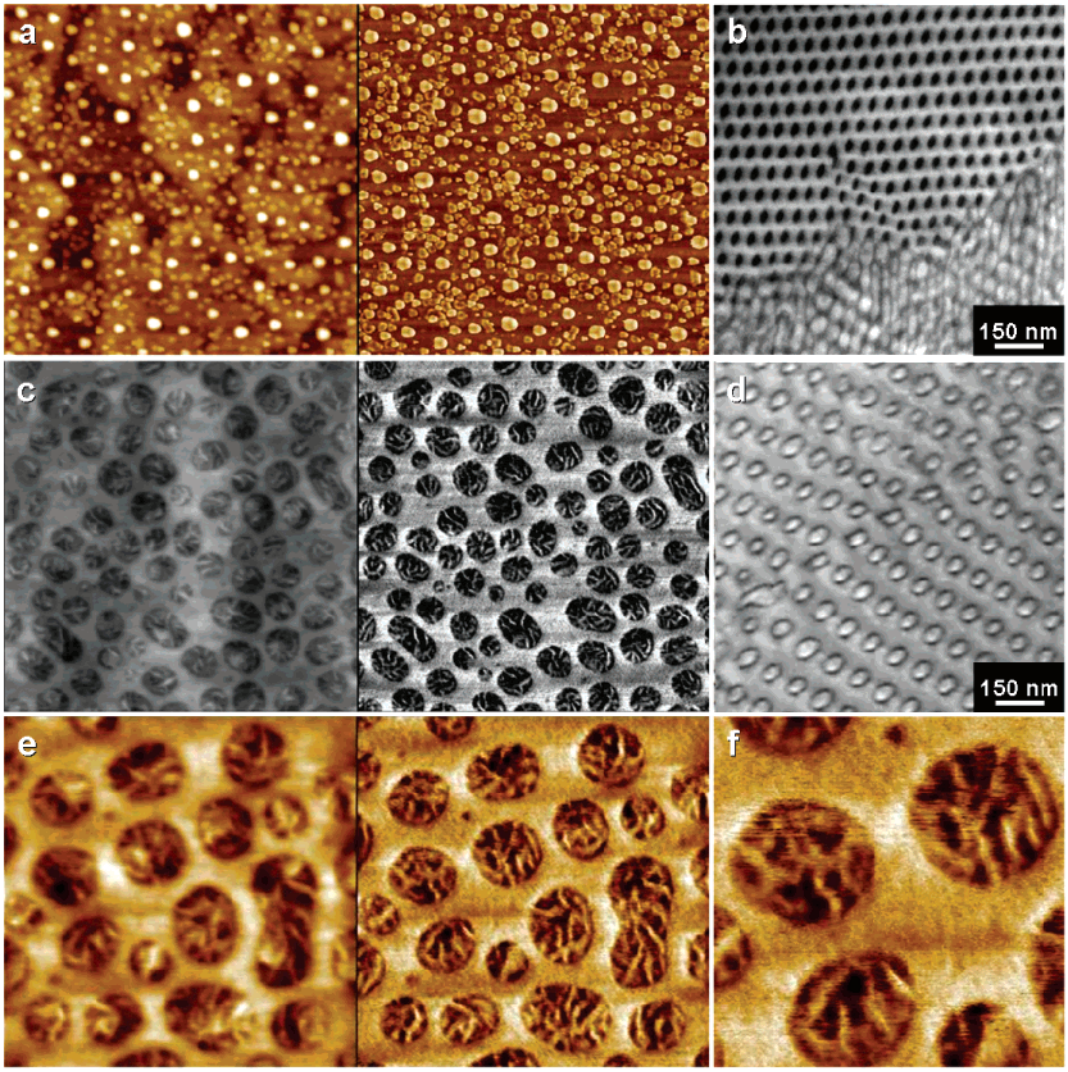

Figure 1. AFM height (left) and phase (right) images, 1 μm × 1 μm, with $z_{max,height}$ = 20 nm, and TEM micrographs of ultrathin sections. (a) AFM image and (b) TEM micrograph of $B_{17}S_{68}EO_{16}^{210}$. (c) AFM image and (d) TEM micrograph of $E_{17}S_{67}EO_{16}^{211}$. (e) AFM image of $E_{17}S_{67}EO_{16}^{211}$, 500 nm × 500 nm, and (f) zoom-in of the phase image in (e).

It is evident from the results presented in Figure 1 that the thin film morphology is similar to the bulk morphology (TEM micrographs are shown in Figure 1b,d; SAXS scattering patterns have shown an fcc-packed spheres structure, as published elsewhere).[39] However, the long-range order obtained in the spin-coated film is not as good as the one observed in the cast film used for studies of the behavior in the bulk. This relates to the lower mobility of the polymer chain in the thin film, caused by the interaction forces with the substrate.

To completely define the morphology in the hydrogenated triblock terpolymer, it is necessary to be able to distinguish the polyethylene crystals from the poly(ethylene oxide) crystals. For this purpose, the thin film sample was subjected to swelling in water for 30 min. Water is a solvent only for the poly(ethylene oxide) block but a nonsolvent for polyethylene and polystyrene blocks. Therefore, it is expected that only the poly(ethylene oxide) domains swell. The result of such experiment is presented in Figure 2.

The height and phase images presented in Figure 2 give insight into the morphology of the triblock terpolymer. It is possible to locate the poly(ethylene oxide) domains as the swollen circular domains in Figure 2b, since they are bumps in the height image and are soft areas in the phase image (the nonswollen film is presented in Figure 2a for the sake of comparison). The swollen (or partially dissolved) PEO block can only expand toward the top of the polymer film and covers

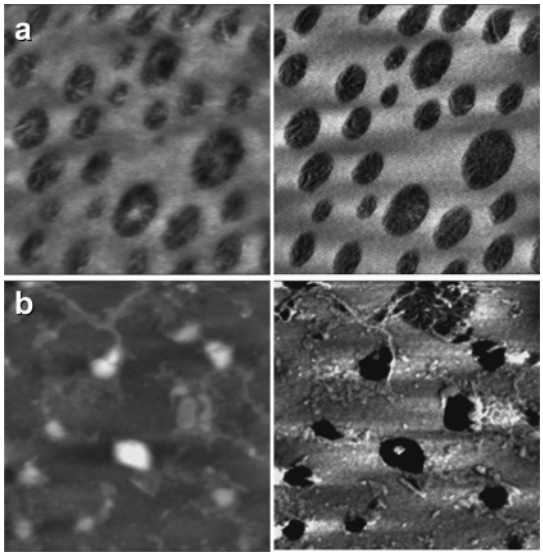

Figure 2. AFM height (left) and phase (right) images of $E_{17}S_{67}EO_{16}^{211}$ (1 μm × 1 μm, with $z_{max,height}$ = 20 nm) (a) before and (b) after swelling 30 min with water.

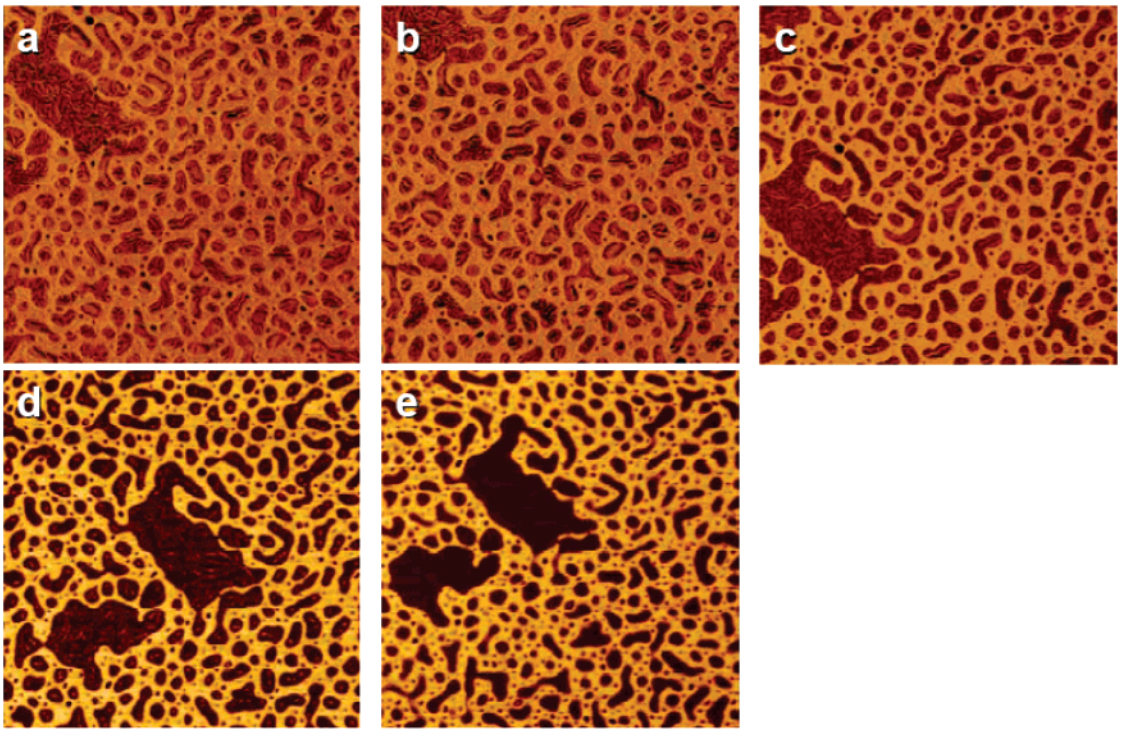

Figure 3. AFM phase images for $E_{17}S_{67}EO_{16}^{211}$ (2 μm × 2 μm, with $z_{max,phase}$ = 100°) during a heating protocol. (a) T = 25 °C, (b) T = 50 °C, (c) T = 75 °C, (d) T = 100 °C, (e) T = 110 °C.

therefore the PE lamellae observed previously. Only one of the circular domains does not seem to contain a significant amount of poly(ethylene oxide) in the 1 μm^2 area shown. This could indicate that both polyethylene and poly(ethylene oxide) blocks share the circular domains in most of the cases. Also, this method allowed the identification of a few PEO chains dispersed in the PS matrix, given the mobility restrictions associated with such high molecular weight and substrate interactions that evidence that the obtained morphologies could not be completely in equilibrium.

Now that the poly(ethylene oxide) block has been located in the observed thin film morphology thanks to the water swelling experiments, heating experiments have been conducted on $E_{17}S_{67}EO_{16}^{211}$, in order to identify also the polyethylene block. The initial concentration of the polymer solution was 9 mg/mL, so the thin films here presented are slightly thinner than the ones presented before. Phase images of a heating sequence are shown in Figure 3, and the subsequent cooling is presented in Figure 4.

The initial morphology shown in Figure 3a is very similar to the one presented before (see Figure 1c) although in this case some domains are evidently bigger than others. It is possible to follow the beginning of the melting at 75 °C (Figure 3c) while most of the polyethylene crystals remain. It is worth noting that this temperature is above the maximum possible melting point of the PEO block, as derived from differential scanning calorimetry (DSC) experiments published elsewhere.[39] At 100 °C (Figure 3d) some polyethylene crystals melt, but the complete melting is seen only at 110 °C (Figure 3e). The polyethylene crystals remaining above 75 °C can be observed in all the circular domains. Since the PEO block was identified in virtually every domain during the water-swelling experiments and the PE lamellae were found in every domain above 75 °C during the heating experiments, it is therefore confirmed that the two blocks PE and PEO share the confined domains in this morphology within the studied temperature range.

The crystallization from the melt can be analyzed from the results shown in Figure 4. A small amount of crystallization is already observed at 100 °C (Figure 4b) in the bigger domains, where the crystals are observed to grow at the domain interface, as was already seen in Figure 1f. From thermal studies carried out in bulk samples, the crystallization temperatures of the two blocks were determined by DSC as $T_{c,PE}$ = 55.9 °C and $T_{c,PEO}$ = −30.9 °C.[39] Those are average values, and it comes as no surprise that the onset of PE crystallization is observed at 100 °C. The sample at 50 °C (Figure 4e) looks as it has reached (or it is close to) the highest crystallization degree possible under the given conditions. Because of the low crystallization temperature of the PEO block, it is only expected to undergo crystallization under very large supercoolings, which were not achieved during the presented experiment. Only temperatures well below room temperature or long storage times will allow the crystallization. Therefore, the observed lamellae are exclusively PE crystals, and the PEO block forms an amorphous phase inside the domains, depicted as the darker areas since it appears as a low AFM phase material.

As was already mentioned, the PE and the PEO blocks are sharing the disklike domains in the temperature range studied, i.e., from room temperature to the melting point of the PE block. (Further experiments and analysis regarding the molten state were not carried out, and they are beyond the scope of the present contribution.) The tendency of the two blocks to segregate is expected, since the segmental interaction parameter has a value of 0.16 at 60 °C,[52,57,58] and it is the largest among all the possible pairs.[39] However, it seems that certain particularities of the system, such as the low content of crystalline blocks, low molecular weight of the crystallizable blocks compared to the PS block, surface interaction, and restriction arising from the solvent employed (toluene is a very good solvent for PS, a nonideal solvent for PEO, and a poor solvent for PE) and from crystallization, allow the formation of such shared domains in a case of otherwise immiscible blocks. It

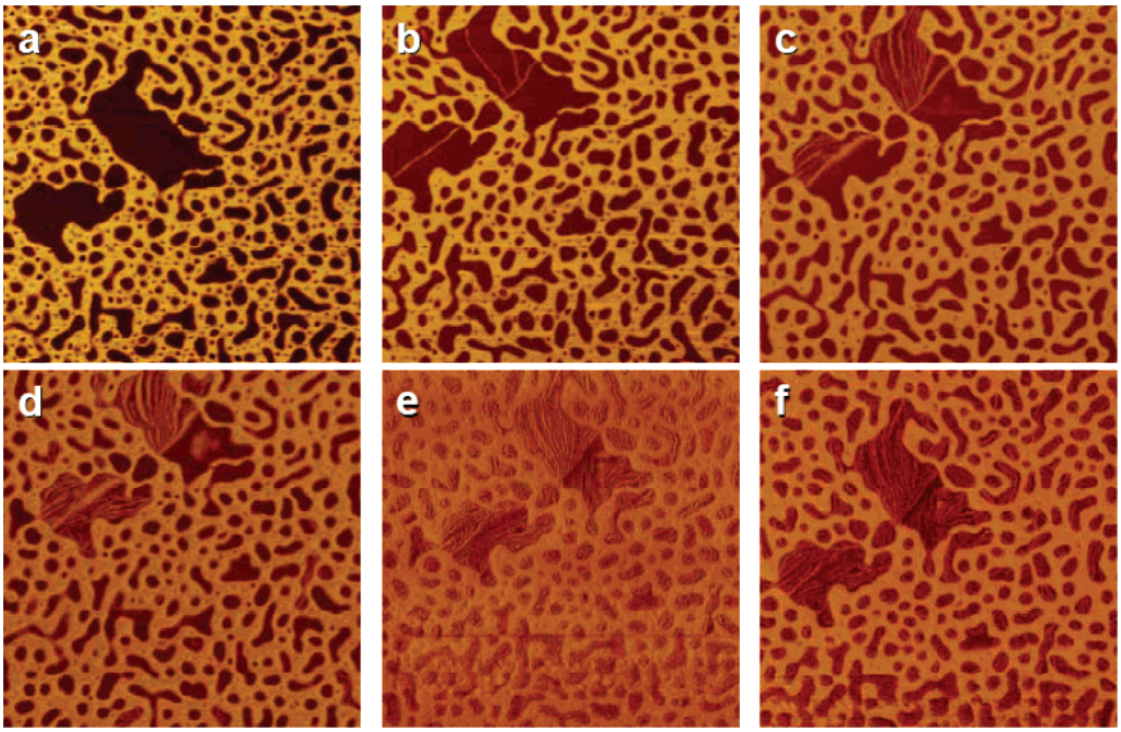

Figure 4. AFM phase images for $E_{17}S_{67}EO_{16}^{211}$ (2 μm × 2 μm, with $z_{max,phase}$ = 100°) during a cooling protocol. (a) T = 110 °C, (b) T = 100 °C, (c) T = 90 °C, (d) T = 75 °C, (e) T = 50 °C, (f) T = 25 °C.

has been observed that polymer crystallization is able to overcome miscibility driven phase behavior, as it can produce fractionation of chemically identical polymer chains as a function of their molecular weight, caused by molecular weight dependent crystallization kinetics and melting temperatures.[36,50,59,60]

Further experiments on the thin film morphology of $E_{17}S_{67}EO_{16}^{211}$ were carried out by employing different polymer solution concentrations for the film preparation. In Figure 5, the AFM images of films prepared from 5.0, 7.5, and 10.0 mg/mL polymer solutions are presented. This variation in solution concentration reflects in the final film thickness, since all other spin-coating parameters were kept constant.

The results in Figure 5 show significant changes of the morphology with the film thickness. The thinnest film, i.e., the film prepared from a 5.0 mg/mL solution presented in Figure 5a, shows wormlike domains that are higher in topography than the matrix. Given the triblock terpolymer composition as well as the previous results, these domains are formed by the PE and the PEO blocks. The two blocks form spherical domains in bulk (Figure 1d), but since the film thickness limits one of the dimensions, they are not spherical but stretched to the observed wormlike domains. In the phase image it is possible to observe features inside the domains, which should correspond to the crystalline PE phase, although they are not very well-defined.

The film prepared from a 7.5 mg/mL solution (Figure 5b) shows a morphology where the domains are even more deformed than in the thinnest film. The presented features correspond to a coalescence of the PE/PEO domains to form bigger ones. The chain dimensions are presented in Table 2, calculated for the extended chain and the unperturbed coil of each block. The dimensions presented for the PS block fit with the interdomain distances observed in the AFM images. The circular, not merged, domains also have dimensions in good agreement with the PE and PEO chain dimensions. The merged domains are, on the contrary, too big compared to the chains,

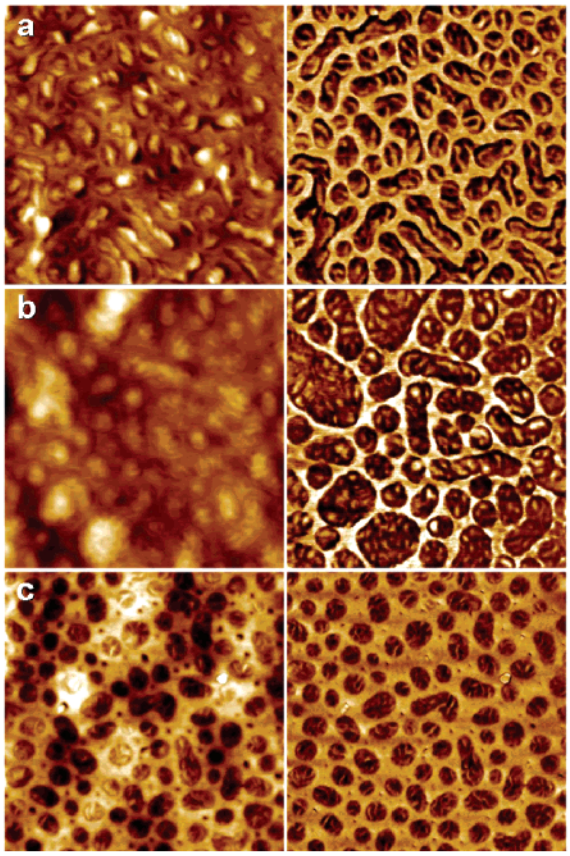

Figure 5. AFM height (left) and phase (right) images of $E_{17}S_{67}EO_{16}^{211}$ (1 μm × 1 μm, with $z_{max,height}$ = 10 nm, $z_{max,phase}$ = 30°, tapping softly on the surface) of films prepared by spin-coating from (a) 5.0, (b) 7.5, and (c) 10.0 mg/mL polymer solutions in toluene.

and therefore such domains should be interpreted as flat domains on the surface "filled" with end blocks of terpolymer chains that lie underneath them.

Table 2. All-Trans Conformation (L') and Unperturbed Coil ($2\langle s^2\rangle_{real}^{1/2}$) Chain Dimensions of the Blocks in $E_{17}S_{67}EO_{16}^{211}$

block	L' (nm)	$2\langle s^2\rangle_{real}^{1/2}$ (nm)
polyethylene	80.9	16.8
polystyrene	171.8	29.8
poly(ethylene oxide)	93.4	13.4

The observed morphology changes drastically for the thickest film, which is shown in Figure 5c. The PE/PEO domains form depressions instead of bumps in the height image, the inner-domain structure shown in the phase image corresponds to crystalline lamellae, the size of the domains has decreased, and their shape is more spherical. In summary, the morphology is more similar to the bulk morphology observed by TEM than in any other case. It can be assumed that the film thickness obtained with a 10.0 mg/mL polymer solution is enough to allow the formation of spherical domains similar to those formed in bulk. Still, some domains have merged together, and the long-range order is not as good as in bulk. The merge of the domains observed in different thin films explains the big domains found in Figures 3 and 4.

Additional information on the morphology is given by using different tapping forces to image the sample surface. The corresponding results are presented in Figure 6, with the images obtained by soft (Figure 6a) and hard (Figure 6b) tapping. While the overall morphology is similar to what has been discussed so far, some interpretations can be introduced.

In the phase image obtained by soft tapping on the surface (Figure 6a), it is possible to see the stiff PE lamellae inside the circular domains, surrounded and intercalated by soft PEO and PE amorphous phase. (Figure 4 is consistent with previous calorimetry results where the PEO block did not crystallize at the temperatures employed in the present experiments.) By increasing the tapping force (Figure 6b), the matrix is better defined as a stiff material, which supports the assumption that the matrix consists of PS. Also, the stiff PE lamellae inside the domains seem to cover less area than in Figure 6a. This could be the effect of some rearrangement caused by the tip that pushes hard toward the substrate. Most likely, the PE lamellae are sunk into the amorphous PEO domains. Some of the smaller lamellae could also have lost their flat-on orientation and reorient to edge-on.

A 3-D representation of the topography obtained by soft tapping is presented in Figure 6c. The PE/PEO domains are observed as bumps on the surface, which has not always been the case in the previously presented images. This could be an effect of the aging of the sample, since the long time storage has allowed the PEO crystallization. However, this was not identified in all the aged $E_{17}S_{67}EO_{16}^{211}$ samples and therefore cannot be 100% attributed to PEO crystallization. As a matter of fact, most of the aged samples of $E_{17}S_{67}EO_{16}^{211}$ look unchanged.

Effect of Annealing Procedures on the Morphology. In order to study the effect of the thermal treatment on the morphology of the triblock terpolymer, crystallization of $E_{17}S_{67}EO_{16}^{211}$ was carried out at different thermal conditions. The sample was spin-coated from the 10 mg/mL toluene solution and immediately melted at 200 °C. Further, it was quenched to a T_c and kept there for the crystallization time. In some cases, two different T_cs were used in sequence, in order to crystallize first the polyethylene block and later the poly(ethylene oxide) block. The AFM height and phase images as well as the conditions used during sample preparation are described in Figure 7. In order to gain more insight into the influence of

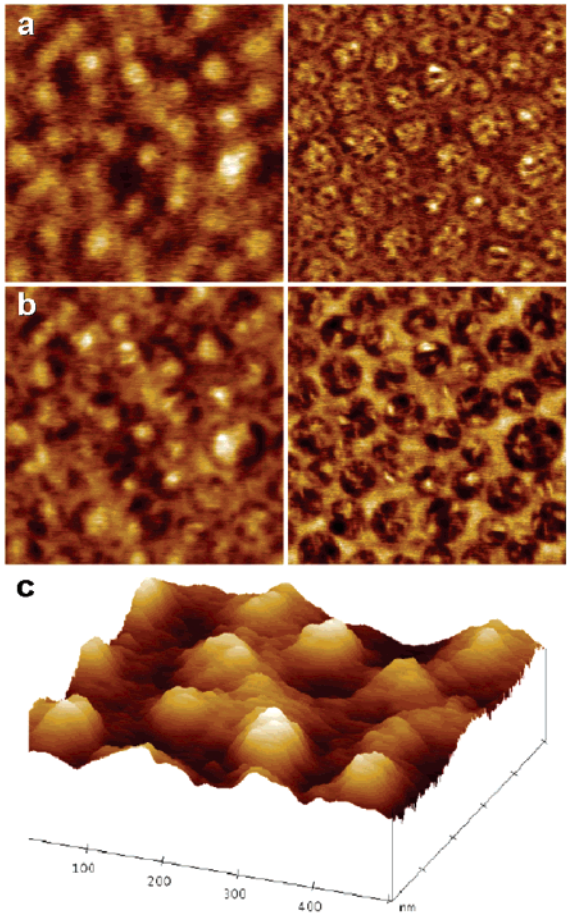

Figure 6. AFM height (left) and phase (right) image of $E_{17}S_{67}EO_{16}^{211}$ (1 μm × 1 μm) obtained by (a) soft tapping and (b) hard tapping on the surface. (c) 3-D representation of a zoom-in area into the height image in (a), with $z_{max,height} = 3$ nm.

crystallization condition on the microphases, one of these samples (Figure 7d) was further submitted to a thermal treatment below T_m of the PE block in order to anneal the already existent crystals. The results are shown in Figure 7f.

It is evident from Figure 7 that some changes in the microphases occur when the sample is subjected to different crystallization programs. In order to quantify these effects, the images were analyzed and the average diameter of the disks was calculated. The disk diameter distribution was then fitted to a Gaussian distribution (results not shown), and the mean disk diameter values were obtained. The results from fittings made to images in Figure 7 are represented in Figure 8 as disk diameter as a function of the first crystallization temperature used in the thermal treatment. The value corresponding to the sample with further crystal annealing (Figure 7f) is plotted for direct comparison.

In Figure 8, the tendency of in the thermal treatment on the disk diameter can be seen. The sample treated at 65 °C (shown in Figure 7c) presented a low disk diameter, which we attribute to the short holding time at the crystallization temperature. For the sample annealed after the crystallization treatment (Figure 7f), the diameter shows an increase compared to the nonannealed one. This result is comparable to the increase of lamellar thickness with crystallization temperature and with crystal annealing below T_m. It is fascinating that the actual size of the domain is also affected in the same way. The crystals are thicker and the density inside the domain is therefore higher at higher crystallization temperatures, from where one would usually assume a smaller domain. However, a higher holding temper-

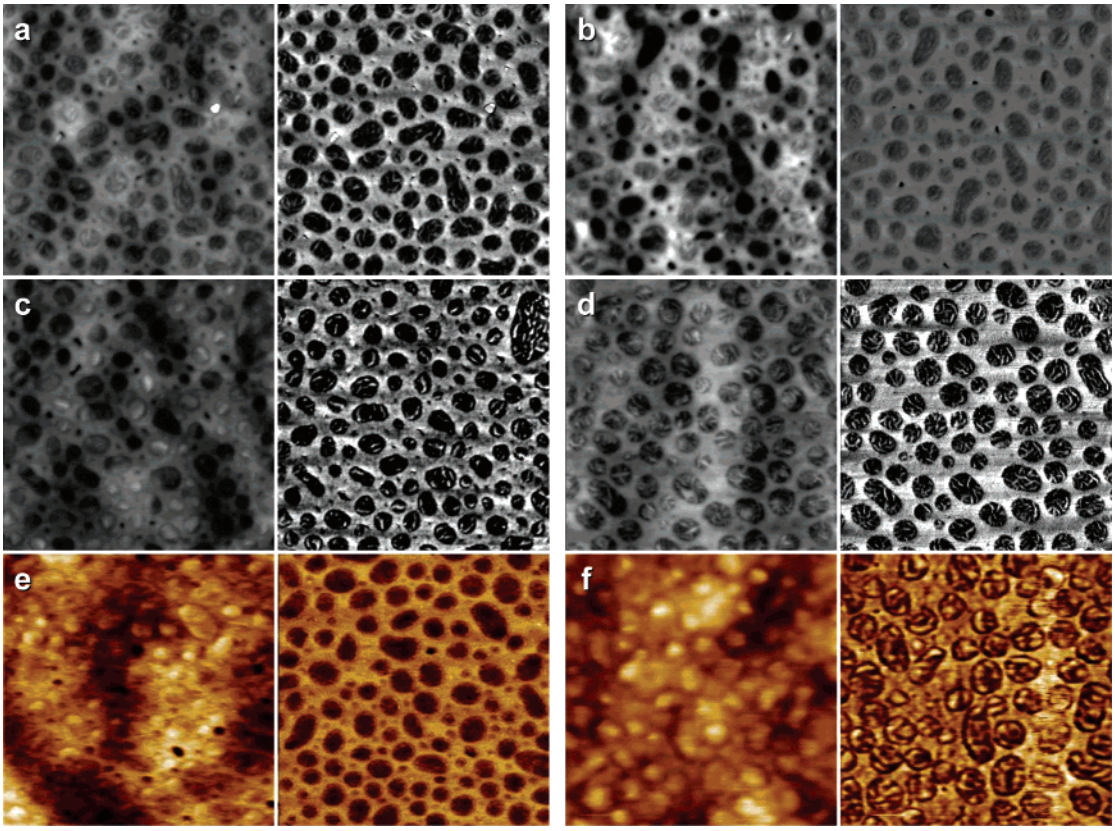

Figure 7. AFM height (left) and phase (right) image of $E_{17}S_{67}EO_{16}^{211}$ (1 μm × 1 μm, with $z_{max,height}$ = 20 nm) melted 60 min at 200 °C and then crystallized with the following procedure: (a) 4205 min at −26 °C, (b) 4030 min at 0 °C, (c) 300 min at 65 °C, followed by 3770 min at −26 °C, (d) 1059 min at 70 °C, followed by 1445 min at 0 °C, (e) 440 min at 80 °C, followed by 840 min at −26 °C, (f) 1059 min at 70 °C and 1445 min at 0 °C, followed by annealing 842 min at 80 °C.

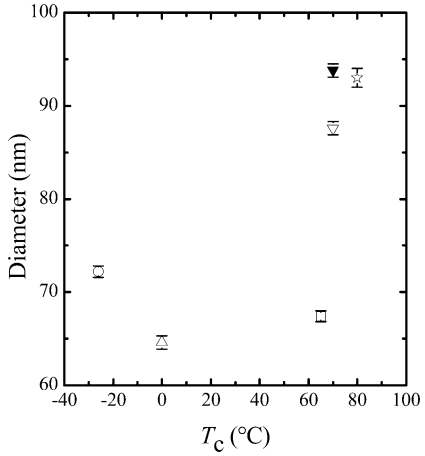

Figure 8. Disk diameter distribution for $E_{17}S_{67}EO_{16}^{211}$ as a function of the higher crystallization temperature used in the thermal treatment (PE crystallization temperature). The data correspond to the images shown in Figure 7, as follows: samples melted 60 min at 200 °C and then crystallized with the following procedure: (○) 4205 min at −26 °C; (△) 4030 min at 0 °C; (□) 300 min at 65 °C, followed by 3770 min at −26 °C; (▽) 1059 min at 70 °C, followed by 1445 min at 0 °C; (☆) 440 min at 80 °C, followed by 840 min at −26 °C; (▼) 1059 min at 70 °C and 1445 min at 0 °C, followed by annealing 842 min at 80 °C.

ature also implies higher mobility of the overall chain, and in consequence a more uniform microphase separation arrangement. This increased mobility for long time allows that more short chains come inside the confined domains, making them bigger than before the treatment. (The presence of short PEO chains dispersed in the matrix was already revealed by the swelling experiments.) These results evidence that the structures obtained at room temperature depend on crystallization and annealing conditions.

Even though theoretically the equilibrium morphology could be reached after very long annealing at high temperatures, in practice this state is very difficult to reach experimentally due to slow dynamics of the high molecular weights and the risk of degradation of the PEO block. Therefore, the present study focuses mainly on the influence of the particular morphology of a triblock terpolymer system on crystallization. However, many questions regarding the morphology of the molten state remain, such as whether the PE and the PEO would ever segregate and how the phase segregation is in the equilibrium morphology.

The results summarized in Figure 8 indicate the possibility to control the dimensions of the spherical crystalline microphases by means of the thermal protocol applied to the sample, as has been previously found in block copolymers by a different technique.[36] The diameter of the spherical microphases can be increased up to 30% using the same triblock terpolymer. This means that no time-consuming new synthesis is needed in order to vary the spherical size by changing the composition or the molecular weight, opening new possibilities in the control of microphase separation and morphology generation.

The study of the thickness of the crystalline lamellae as a function of the different annealing treatments was not carried out since the error associated with the measurements is not quantifiable. The observed thickness of the crystalline lamellae has been seen to depend on the tapping force (Figure 6b), and even when all measurements are taken under "soft tapping" conditions, the force still varies inevitably from sample to sample.

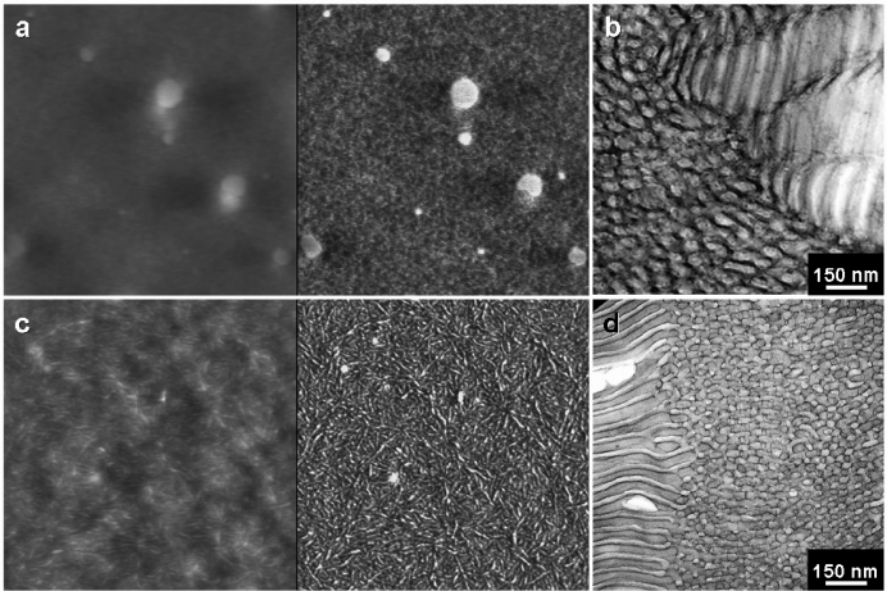

Figure 9. AFM height (left) and phase (right) images, 1 μm × 1 μm, with $z_{max,height}$ = 20 nm, and TEM micrographs of ultrathin sections. (a) AFM image and (b) TEM micrograph of $B_{29}S_{40}EO_{31}^{168}$. (c) AFM image and (d) TEM micrograph of $E_{29}S_{40}EO_{31}^{170}$.

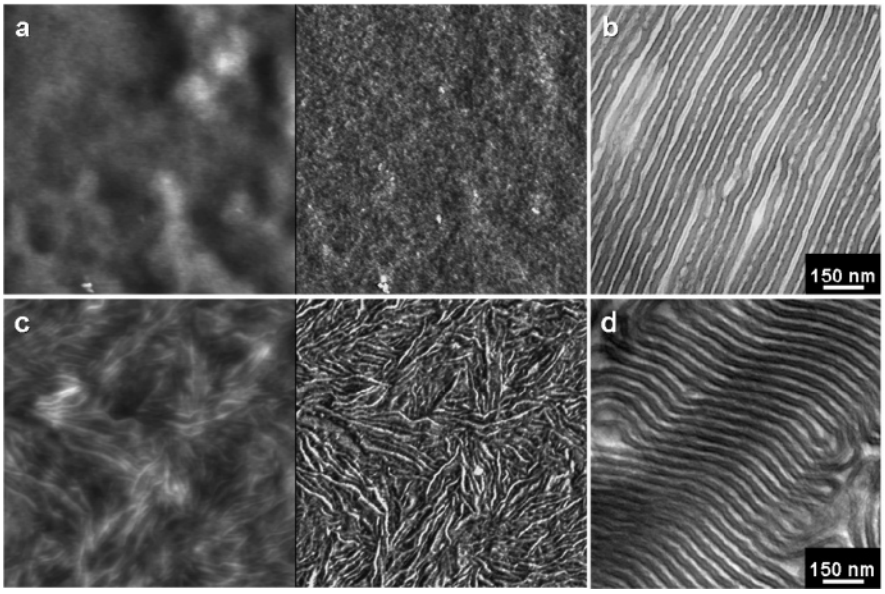

Figure 10. AFM height (left) and phase (right) images, 1 μm × 1 μm, with $z_{max,height}$ = 20 nm, and TEM micrographs of ultrathin sections. (a) AFM image and (b) TEM micrograph of $B_{37}S_{16}EO_{47}^{76}$. (c) AFM image and (d) TEM micrograph of $E_{38}S_{16}EO_{46}^{77}$.

Morphology of Triblock Terpolymers with Different Compositions. The morphology of triblock terpolymers with two other compositions has been studied. These two cases are terpolymers also with similar content of PE and PEO end blocks, where the PS content is decreased (the content of the crystallizable blocks is increased). This change in composition causes two main effects: first, the self-assembled morphology obtained varies from spherical domains to cylinders and lamellae, and second, the PEO block is able to crystallize at room temperature.

The morphology of $B_{29}S_{40}EO_{31}^{168}$ and its hydrogenated triblock terpolymer is presented in Figure 9. The height images (Figure 9a,c) show that the film prepared is relatively flat, with z_{max} < 20 nm. From the phase image of the non-hydrogenated terpolymer shown in Figure 9a, the dark dispersed polybutadiene domains can be identified, as well as a gray-featured polystyrene matrix. The poly(ethylene oxide) crystals are not evident, which means the block is not preferentially located at the surface but toward the substrate (completely amorphous PEO is not expected on the basis of calorimetry results that showed T_c = 37.9 °C).[39] The ordered structure observed in bulk by TEM (Figure 9b) was not observed in the thin film. Increases of the AFM tapping strength did not reveal any different features. In the case of the hydrogenated terpolymer ($E_{29}S_{40}EO_{31}^{170}$) displayed in Figure 9c, the crystal lamellae are evident, as well as some circular crystalline features that could be interpreted as cylinders, which relates well with the bulk morphology presented in Figure 9d.

The thin film morphology results for the third pair of triblock terpolymers studied here, $B_{37}S_{16}EO_{47}^{76}$ and $E_{38}S_{16}EO_{46}^{77}$, are summarized in Figure 10. As has been shown for the previous terpolymers, Figure 10a shows the AFM phase image of a thin film of the non-hydrogenated $B_{37}S_{16}EO_{47}^{76}$, where the poly(ethylene oxide) crystalline lamellae were not evident even after increasing the tapping force during the measurement. The bulk morphology (Figure 10b) was also not obtained in the thin film.

The thin film morphology of $E_{38}S_{16}EO_{46}^{77}$ shows crystalline lamellae (Figure 10c), supposedly of both polyethylene and poly(ethylene oxide) blocks. Compared to the previous results,

in this material it is possible to observe more crystalline features than in the others. This is expected since the content of crystallizable blocks (polyethylene and poly(ethylene oxide)) in the triblock terpolymer is around 84 wt %, compared to 60 and 32 wt % from the other two cases. The bulk morphology (Figure 10d) has been determined as a clear lamellae morphology,[39] but it is not possible to distinguish the long-range ordered microphases in the AFM images.

The results presented in this section evidence discrepancies between the thin film morphology and the bulk morphology already established[39] by microscopy (TEM) and small-angle X-ray scattering (SAXS) for the systems with continuous crystalline phases. Variations in polymer solution concentration and tapping force did not provide any information different from the one presented here. Further experiments such as film preparation from different solvents or onto different substrates could give deeper understanding of the morphology and the influence of crystallization in continuous phases.

Conclusions

The thin film morphology of $E_{17}S_{67}EO_{16}^{211}$ was studied by atomic force microscopy. The technique provided successful identification and differentiation of polyethylene and poly(ethylene oxide) blocks in the observed morphology. This was possible by studying the surfaces after swelling the poly(ethylene oxide) block with a selective solvent and during heating the sample beyond its melting temperature. Dispersed spherical domains shared by polyethylene crystals and amorphous poly(ethylene oxide), which are usually segregated, were found for $E_{17}S_{67}EO_{16}^{211}$. The size and shape of those domains varied from wormlike to wide flat domains to spherical ones with the film thickness. The dimensions of the spherical or disklike domains could be controlled by adjusting the temperature program applied to the sample. The thin film morphologies of two different compositions with higher content of the crystalline blocks were also studied and showed continuous crystalline lamellae at the surface, in contrast to the lamellae confined in dispersed domains observed in $E_{17}S_{67}EO_{16}^{211}$.

Acknowledgment. The authors thank C. Abetz (GKSS Research Centre Geesthacht GmbH) and A. Gödel (University of Bayreuth) for the TEM measurements. The support from Dr. H. Stadler (Veeco Instruments) is highly appreciated. Financial support was partially given by the European Action COST P12.

References and Notes

(1) Bates, F. S. *Science* **1991**, *251*, 898−905.
(2) Lodge, T. P. *Macromol. Chem. Phys.* **2003**, *204*, 265−273.
(3) Hamley, I. W. *The Physics of Block Copolymers*; Oxford University Press: Oxford, 1998.
(4) Abetz, V.; Stadler, R. *Macromol. Symp.* **1997**, *113*, 19−26.
(5) Bates, F. S. F.; Glenn, H. *Phys. Today* **1999**, *52*, 32−38.
(6) Bucknall, D. G.; Anderson, H. L. *Science* **2003**, *302*, 1904−1905.
(7) Choi, S.; Lee, K. M.; Han, C. D.; Sota, N.; Hashimoto, T. *Macromolecules* **2003**, *36*, 793−803.
(8) Hamley, I. W. *Nanotechnology* **2003**, *14*, R39.
(9) Jeong, U.; Lee, H. H.; Yang, H.; Kim, J. K.; Okamoto, S.; Aida, S.; Sakurai, S. *Macromolecules* **2003**, *36*, 1685−1693.
(10) Jiang, S.; Göpfert, A.; Abetz, V. *Macromolecules* **2003**, *36*, 6171−6177.
(11) Li, L.; Serero, Y.; Koch, M. H. J.; de Jeu, W. H. *Macromolecules* **2003**, *36*, 529−532.
(12) Ruzette, A.-V.; Leibler, L. *Nat. Mater.* **2005**, *4*, 19−31.
(13) Sota, N.; Sakamoto, N.; Saijo, K.; Hashimoto, T. *Macromolecules* **2003**, *36*, 4534−4543.
(14) Stupp, S. I.; LeBonheur, V.; Walker, K.; Li, L. S.; Huggins, K. E.; Keser, M.; Amstutz, A. *Science* **1997**, *276*, 384−389.
(15) Sundrani, D.; Darling, S. B.; Sibener, S. J. *Nano Lett.* **2004**, *4*, 273−276.
(16) Whitesides, G.; Mathias, J.; Seto, C. *Science* **1991**, *254*, 1312−1319.
(17) Zhu, L.; Cheng, S. Z. D.; Huang, P.; Ge, Q.; Quirk, R. P.; Thomas, E. L.; Lotz, B.; Hsiao, B. S.; Yeh, F.; Liu, L. *Adv. Mater.* **2002**, *14*, 31−34.
(18) Zhu, Y.; Gido, S. P.; Iatrou, H.; Hadjichristidis, N.; Mays, J. W. *Macromolecules* **2003**, *36*, 148−152.
(19) Bockstaller, M. R.; Lapetnikov, Y.; Margel, S.; Thomas, E. L. *J. Am. Chem. Soc.* **2003**, *125*, 5276−5277.
(20) Förster, S.; Antonietti, M. *Adv. Mater.* **1998**, *10*, 195−217.
(21) Lazzari, M.; López-Quintela, M. A. *Adv. Mater.* **2003**, *15*, 1583−1594.
(22) Park, C.; Yoon, J.; Thomas, E. L. *Polymer* **2003**, *44*, 6725−6760.
(23) Aizawa, M.; Buriak, J. M. *J. Am. Chem. Soc.* **2005**, *127*, 8932−8933.
(24) Cao, D.; Wu, J. *Macromolecules* **2005**, *38*, 971−978.
(25) Feng, C. L.; Embrechts, A.; Vancso, G. J.; Schonherr, H. *Eur. Polym. J.* **2006**, *42*, 1954−1965.
(26) Cheng, J. Y.; Ross, C. A.; Thomas, E. L.; Smith, H. I.; Vancso, G. J. *Appl. Phys. Lett.* **2002**, *81*, 3657−3659.
(27) Ouk Kim, S.; Solak, H. H.; Stoykovich, M. P.; Ferrier, N. J.; de Pablo, J. J.; Nealey, P. F. *Nature (London)* **2003**, *424*, 411−414.
(28) Müller, A. J.; Balsamo, V.; Arnal, M. L. In *Lecture Notes in Physics: Progress in Understanding of Polymer Crystallization*; Reiter, G., Strobl, G., Eds.; Springer: Berlin, 2007; pp 229−259.
(29) Chen, H.-L.; Hsiao, S.-C.; Lin, T.-L.; Yamauchi, K.; Hasegawa, H.; Hashimoto, T. *Macromolecules* **2001**, *34*, 671−674.
(30) Huang, E.; Rockford, L.; Russell, T. P.; Hawker, C. J. *Nature (London)* **1998**, *395*, 757−758.
(31) Reiter, G.; Castelein, G.; Sommer, J.-U. Crystallization of Polymers in Thin Films: Model Experiments. In *Lecture Notes in Physics: Polymer Crystallization: Observations, Concepts and Interpretations*; Reiter, G., Sommer, J.-U., Eds.; Springer: Berlin, 2003; Vol. 606, pp 131−152.
(32) Zhu, L.; Huang, P.; Chen, W. Y.; Ge, Q.; Quirk, R. P.; Cheng, S. Z. D.; Thomas, E. L.; Lotz, B.; Hsiao, B. S.; Yeh, F.; Liu, L. *Macromolecules* **2002**, *35*, 3553−3562.
(33) Zhu, L.; Chen, H.-L.; Calhoun, B. H.; Ge, Q.; Quirk, R. P.; Thomas, E. L.; Hsiao, B. S.; Yeh, F.; Lotz, B. *Polymer* **2001**, *42*, 5829−5839.
(34) Zhu, L.; Chen, Y.; Zhang, A.; Calhoun, B. H.; Chun, M.; Quirk, R. P.; Cheng, S. Z.; Hsiao, B. S.; Yeh, F.; Hashimoto, T. *Phys. Rev. B* **1999**, *60*, 10022−10031.
(35) Cohen, R. E.; Cheng, P.-L.; Douzinas, K.; Kofinas, P.; Berney, C. V. *Macromolecules* **1990**, *23*, 324−327.
(36) Lorenzo, A. T.; Arnal, M. L.; Müller, A. J.; Boschetti-de-Fierro, A.; Abetz, V. *Eur. Polym. J.* **2006**, *42*, 516−533.
(37) Takeshita, H.; Ishii, N.; Araki, C.; Miya, M.; Takenaka, K.; Shiomi, T. *J. Polym. Sci., Part B: Polym. Phys.* **2004**, *42*, 4199−4206.
(38) Loo, Y.-L.; Register, R. A. Crystallization within block copolymer mesophases. In *Development in Block Copolymer Science and Technology*; Hamley, I. W., Ed.; John Wiley & Sons: New York, 2004; pp 213−243.
(39) Boschetti-de-Fierro, A.; Müller, A. J.; Abetz, V. *Macromolecules* **2007**, *40*, 1290−1298.
(40) Floudas, G.; Reiter, G.; Lambert, O.; Dumas, P. *Macromolecules* **1998**, *31*, 7279−7290.
(41) Jiang, S.; He, C.; An, L.; Chen, X.; Jiang, B. *Macromol. Chem. Phys.* **2004**, *205*, 2229−2234.
(42) Albuerne, J.; Márquez, L.; Müller, A. J.; Raquez, J. M.; Degée, P.; Dubois, P.; Castelletto, V.; Hamley, I. W. *Macromolecules* **2003**, *36*, 1633−1644.
(43) Müller, A. J.; Albuerne, J.; Esteves, L. M.; Marquez, L.; Raquez, J.-M.; Degée, P.; Dubois, P.; Collins, S.; Hamley, I. W. *Macromol. Symp.* **2004**, *215*, 369−382.
(44) Müller, A. J.; Albuerne, J.; Márquez, L.; Raquez, J.-M.; Degée, P.; Dubois, P.; Hobbs, J.; Hamley, I. W. *Faraday Discuss.* **2005**, *128*, 231−252.
(45) Sun, L.; Lui, Y.; Zhu, L.; Hsiao, B. S.; Avila-Orta, C. A. *Polymer* **2004**, *2004*, 8181−8193.
(46) Hamley, I. W.; Castelletto, V.; Castillo, R. V.; Müller, A. J.; Martin, C. M.; Pollet, E.; Dubois, P. *Macromolecules* **2005**, *38*, 463−472.
(47) Hamley, I. W.; Parras, P.; Castelletto, V.; Castillo, R. V.; Müller, A. J.; Pollet, E.; Dubois, P.; Martin, C. M. *Macromol. Chem. Phys.* **2006**, *207*, 941−953.
(48) Arnal, M. L.; Balsamo, V.; López-Carrasquero, F.; Contreras, J.; Carrillo, M.; Schmalz, H.; Abetz, V.; Laredo, E.; Müller, A. J. *Macromolecules* **2001**, *34*, 7973−7982.
(49) Balsamo, V.; Müller, A. J.; Gyldenfeldt, F. v.; Stadler, R. *Macromol. Chem. Phys.* **1998**, *199*, 1063−1072.
(50) Balsamo, V.; Müller, A. J.; Stadler, R. *Macromolecules* **1998**, *31*, 7756−7763.
(51) Balsamo, V.; Von Gyldenfeldt, F.; Stadler, R. *Macromol. Chem. Phys.* **1996**, *197*, 3317−3341.
(52) Stadler, R.; Auschra, C.; Beckmann, J.; Krappe, U.; Voigt-Martin, I.; Leibler, L. *Macromolecules* **1995**, *28*, 3080−3097.

(53) Takahashi, K.; Hasegawa, H.; Hashimoto, T.; Bellas, V.; Iatrou, H.; Hadjichristidis, N. *Macromolecules* **2002**, *35*, 4859−4861.
(54) Loo, Y.-L.; Register, R. A.; Ryan, A. J. *Macromolecules* **2002**, *35*, 2365−2374.
(55) Magonov, S. N.; Cleveland, J.; Elings, V.; Denley, D.; Whangbo, M.-H. *Surf. Sci.* **1997**, *389*, 201−211.
(56) Boschetti-de-Fierro, A.; Fierro, D.; Albuerne, J.; Funari, S. S.; Abetz, V. *J. Polym. Sci., Part B: Polym. Phys.*, submitted.
(57) Barton, A. F. M. *CRC Handbook of Polymer Liquid Interaction Parameters and Solubility Parameters*; CRC Press: Boca Raton, FL, 1990; p 768.
(58) $\chi = v/RT(\delta_i - \delta_j)^2$, where v is the geometric average of the molar segmental volume calculated from the densities at room temperature (density corrections for the real temperature are neglected) and RT is the molar thermal energy at 60 °C.
(59) Lorenzo, A. T.; Arnal, M. L.; Müller, A. J.; Boschetti-de-Fierro, A.; Abetz, V. *Macromol. Chem. Phys.* **2006**, *207*, 39−49.
(60) Müller, A. J.; Balsamo, V.; Arnal, M. L. *Adv. Polym. Sci.* **2005**, *190*, 1−63.

MA0703812